Quantum Mechanics of the Cooper Pair Box: From Charge Qubit to Transmon

Harry Luo

Physics 531 Final Project, May 2025

1 Introduction

Superconducting circuits containing Josephson junctions provide a platform for building artificial atoms with designable energy spectra, forming the basis of leading quantum computing architectures [2]. The Cooper Pair Box (CPB) is a foundational element, governed by the Hamiltonian:

$$\hat{H} = 4E_C(\hat{N} - n_g)^2 - E_J^{(1)} \cos\hat{\phi} - \frac{E_J^{(2)}}{2}\cos(2\hat{\phi}), \tag{1}$$

where E_C is charging energy, $E_J^{(1,2)}$ Josephson energies, $\hat{N}$ number and $\hat{\phi}$ phase operators ($[\hat{\phi}, \hat{N}] = i$), and n_g gate charge. The ratio E_J/E_C controls the tug-of-war between the E_C term (favoring definite N, localized charge) and the E_J term (favoring definite ϕ, localized phase); the uncertainty principle dictates that localization in one variable implies delocalization in the conjugate variable. A key challenge is sensitivity to n_g fluctuations (charge noise), causing decoherence.

This paper explores how the Hamiltonian (Eq. (1)) in the charging-dominated ($E_C \gg E_J$) and Josephson-dominated ($E_J \gg E_C$) limits lead to different qubit paradigms—the charge qubit and the transmon qubit, respectively—with vastly different sensitivities to this charge noise. We analyze the underlying physical mechanisms and properties, drawing on detailed calculations attached in Appendix A.

2 Charging Dominated Regime & The Charge Qubit

In this limit ($E_J/E_C \ll 1$), neglecting E_J, eigenstates are charge states $|N\rangle$ with energies $E_N^{(0)} = 4E_C(N - n_g)^2$. Because charge N is well-defined, the phase ϕ is completely uncertain ($p(\phi) = 1/(2\pi)$, Appendix A.1), a direct consequence of the uncertainty principle. The physics becomes interesting near points where adjacent charge states are degenerate, most notably at the charge frustration point $n_g = 1/2$, where $E_0^{(0)} \approx E_1^{(0)}$. Here, standard non-degenerate perturbation theory breaks down because energy denominators vanish, and the effect of the Josephson coupling $E_J^{(1)}$ is strongest, mixing the degenerate states. Applying

degenerate perturbation theory within the $\{|0\rangle, |1\rangle\}$ subspace yields the effective Hamiltonian (Appendix A.1):

$$H_{\text{eff}} \approx \epsilon_0 \hat{\sigma}_z - \frac{E_J^{(1)}}{2}\hat{\sigma}_x, \quad \text{where } \epsilon_0 = 4E_C(n_g - 1/2). \tag{2}$$

The resulting energy levels (Fig. 1) show an avoided crossing with minimum gap $E_J^{(1)}$. The linear dependence on $\epsilon_0 \propto (n_g - 1/2)$ leads to extreme sensitivity to gate charge fluctuations, as clearly demonstrated by the sharp transition in ground state charge probability (Fig. 2). This charge noise sensitivity is the primary drawback of the charge qubit. Away from degeneracy (e.g., at $n_g = 0$), standard perturbation theory shows the leading effect of the Josephson coupling is a small second-order energy shift $E_0^{(2)} \approx -(E_J^{(1)})^2/(8E_C)$ (Appendix A.1).

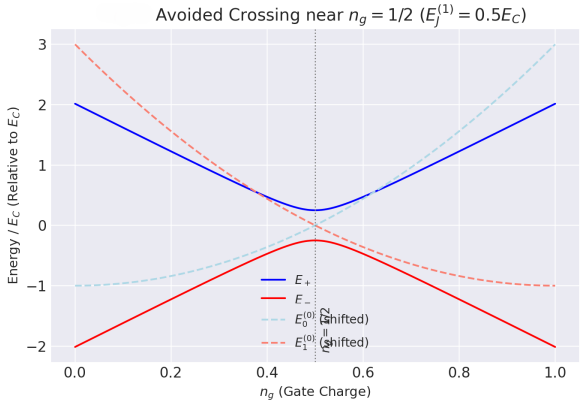

Fig. 1: Avoided crossing near $n_g = 1/2$ (Charge Qubit). Energy levels vs n_g from H_{eff} (Eq. (2)) for $E_J^{(1)} = 0.5E_C$. Shows linear sensitivity. Appendix A.1.

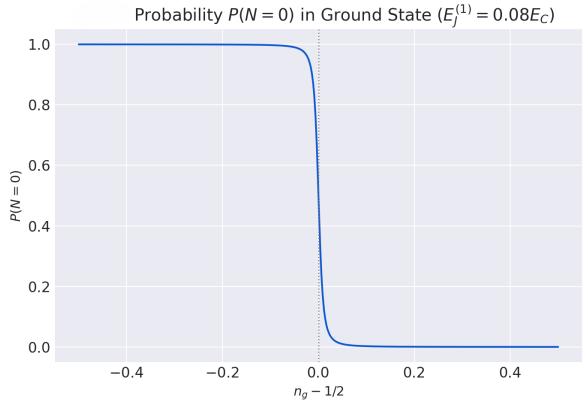

Fig. 2: Ground state probability $P(N = 0)$ near $n_g = 1/2$ for $E_J^{(1)} = 0.08E_C$. Demonstrates extreme n_g sensitivity. Appendix A.1.

3 Josephson Dominated Regime & The Transmon Qubit

In the opposite limit ($E_J \gg E_C$, with $n_g = 0$), the phase ϕ localizes near the potential minimum ($\phi = 0$). The system approximates an anharmonic oscillator (Appendix A.2), with the leading behavior captured by the harmonic Hamiltonian:

$$\hat{H} \approx H_{HO} = V(0) + 4E_C\hat{N}^2 + \frac{1}{2}k\hat{\phi}^2, \tag{3}$$

where $k = E_J^{(1)} + 2E_J^{(2)}$. Phase localization implies charge delocalization; the ground state charge variance $\Delta N^2 = 1/(2X)$, where $X = \sqrt{8E_C/k}$, becomes large (Fig. 3). This signifies immunity to n_g fluctuations as the state averages over many charge numbers.

Crucially, the full cosine potential is anharmonic. Treating the subleading ϕ^4 term as a perturbation to the harmonic oscillator, standard perturbation theory yields corrections to the energy levels characterized by the anharmonicity $\alpha_{anh} = (E_2 - E_1) - (E_1 - E_0)$ (Appendix A.2):

$$\alpha_{anh} \approx -E_C \frac{E_J^{(1)} + 8E_J^{(2)}}{E_J^{(1)} + 2E_J^{(2)}} \approx -E_C. \tag{4}$$

This finite α_{anh} (originating from the subleading potential terms) is essential for selectively addressing the $0 \to 1$ qubit transition without driving higher transitions.

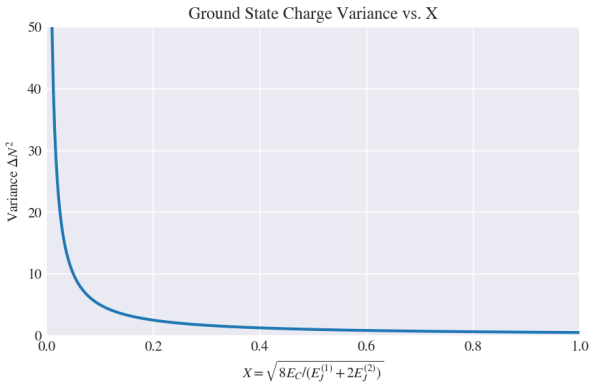

Fig. 3: Ground state charge variance $\Delta N^2 = 1/(2X)$ vs $X = \sqrt{8E_C/k}$. Large variance for large E_J/E_C (small X) signifies charge delocalization, enabling noise immunity. Appendix A.2.

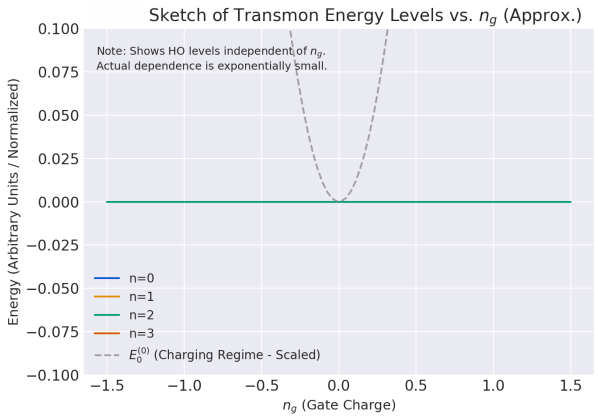

Fig. 4: Conceptual sketch (not to scale): Flat (charge-insensitive) transmon levels ($E_J \gg E_C$, solid) vs parabolic charge qubit levels (dashed $E_0^{(0)}$).

Interpretation: Charge vs. Transmon Synthesis

The distinct physics in the limiting regimes leads to different qubit designs. The **charge qubit** ($E_C \gg E_J$) suffers from its linear sensitivity to n_g (Eq. (2), Figs. 1-2), making it vulnerable to charge noise. The **transmon qubit** ($E_J \gg E_C$) overcomes this by operating with large charge delocalization ($\Delta N^2 \gg 1$, Fig. 3). This provides exponential suppression of n_g sensitivity (charge dispersion), making the transmon robust against charge noise—a significant advantage over the charge qubit. The contrast between these regimes is further illustrated by an exactly solvable case for specific parameters (Appendix A.3). The ground state probability density $p(\phi)$ in this model (Fig. 5) explicitly shows the evolution from a

nearly uniform (charge-like) distribution at low E_J/E_C to one sharply peaked around $\phi = 0$ (transmon-like) at high E_J/E_C, confirming the transition driven by the energy ratio.

This robustness in the transmon regime must be balanced against the need for sufficient anharmonicity ($\alpha_{anh} \approx -E_C$, Eq. (4)) for qubit control. Figure 6 illustrates this trade-off: increasing E_J/E_C exponentially reduces noise sensitivity (panel b) while the necessary anharmonicity quickly saturates near $-E_C$ (panel a), allowing an optimal operating regime (e.g., $E_J/E_C \sim 50$ [1, 2]). The transmon's energy levels become nearly independent of n_g, unlike the charge qubit's parabolic dependence (sketched in Fig. 4).

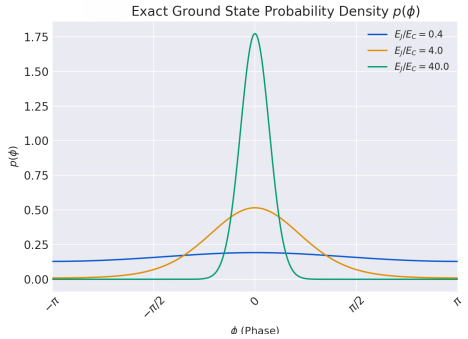

Fig. 5: Exact ground state probability density $p(\phi)$ for the special case, plotted for $E_J/E_C = 0.4, 4.0, 40.0$.

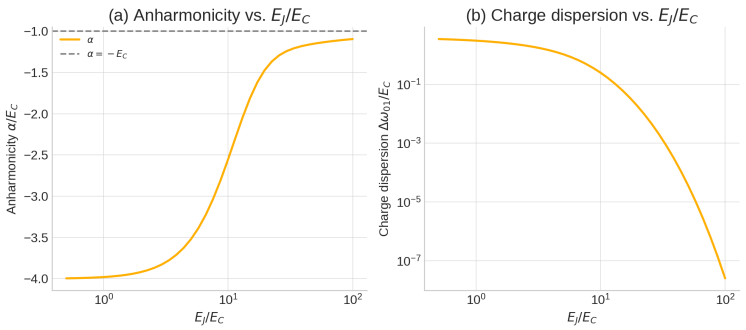

Fig. 6: Transmon trade-off vs E_J/E_C (assuming $E_J = E_J^{(1)}, E_J^{(2)} = 0$). (a) Anharmonicity $\alpha_{anh}/E_C \to -1$. (b) Charge dispersion $\Delta\omega_{01}/E_C$ decays exponentially [1]. Appendix A.2.

4 Conclusion

The quantum behavior of the Cooper Pair Box is fundamentally governed by the ratio E_J/E_C, dictating a transition between charge-dominated and phase-dominated physics. Our analysis contrasted the two resulting qubit paradigms. In the charge qubit regime ($E_C \gg E_J$), the system exhibits energy levels linearly sensitive to the gate charge n_g near degeneracy points, rendering it highly vulnerable to charge noise, as demonstrated by the sharp dependence of charge occupation probability on n_g.

Conversely, the transmon regime ($E_J \gg E_C$) leverages the dominance of Josephson energy to localize the phase ϕ, which, by the uncertainty principle, leads to significant delocalization of the charge state N. This charge delocalization is the key mechanism providing the transmon with exponential immunity to n_g fluctuations, drastically reducing its susceptibility to charge noise compared to the charge qubit. While achieving noise resilience, the transmon retains the essential anharmonicity ($\alpha_{anh} \approx -E_C$) required for qubit addressability. This anharmonicity arises naturally from the higher-order terms of the Josephson cosine

potential, ensuring distinct frequencies for qubit transitions. This favorable combination of charge noise resilience and sufficient anharmonicity for control explains why the transmon has become a robust and widely implemented superconducting qubit architecture.

References

[1] J. Koch, et al., Phys. Rev. A **76**, 042319 (2007).

[2] M. Kjaergaard, et al., Annu. Rev. Condens. Matter Phys. **11**, 369–395 (2020).

A Appendix: Detailed Calculations

Mathematical details supporting the main text results. Units use $\hbar = 1$. We generally retain $E_J^{(1)}$ and $E_J^{(2)}$, but note that often $E_J^{(2)}$ is negligible and E_J is used for $E_J^{(1)}$.

A.1 Part (a): Charging Dominated Regime ($E_C \gg E_J^{(1)}, E_J^{(2)}$)

a.i) Eigenstates, Eigenvalues, and Probability Density ($E_J^{(1,2)} = 0$)

Hamiltonian: $\hat{H}_0 = 4E_C(\hat{N} - n_g)^2$. Eigenstates: $|N\rangle$ such that $\hat{N}|N\rangle = N|N\rangle, N \in \mathbb{Z}$. Eigenvalues:

$$E_N^{(0)}(n_g) = 4E_C(N - n_g)^2$$

These levels are plotted in Figure 7. Phase representation wavefunction: $\psi_N(\phi) = \langle\phi|N\rangle = \frac{1}{\sqrt{2\pi}}e^{iN\phi}$. Probability density: $p_N(\phi) = |\psi_N(\phi)|^2 = 1/(2\pi)$ (uniform).

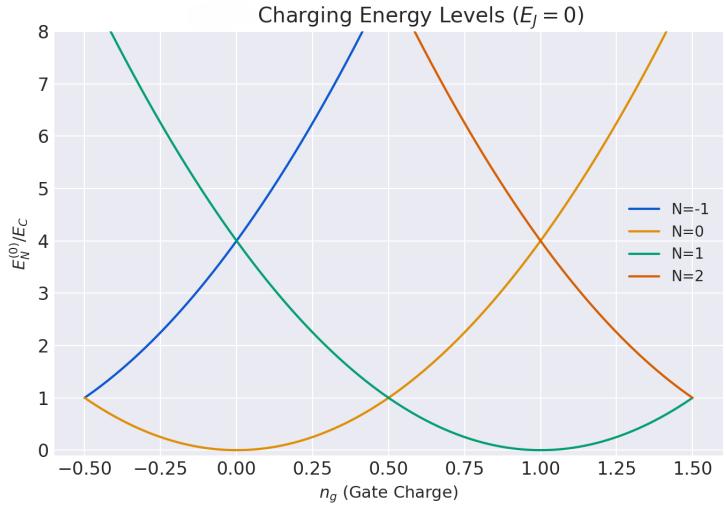

Fig. 7: Charging energy levels $E_N^{(0)}/E_C$ vs n_g for $E_J = 0$.

a.ii) Perturbation Theory Correction at $n_g = 0$

Perturbation: $V = -E_J^{(1)}\cos\hat{\phi} - \frac{E_J^{(2)}}{2}\cos(2\hat{\phi})$. Unperturbed ground state: $|0\rangle$, $E_0^{(0)} = 0$. Valid for $E_J/E_C \ll 1$. First-order correction: $E_0^{(1)} = \langle 0|V|0\rangle = 0$. Second-order correction: $E_0^{(2)} = \sum_{N\neq 0}\frac{|\langle N|V|0\rangle|^2}{E_0^{(0)} - E_N^{(0)}}$. Matrix elements using $\langle N|\cos(k\hat{\phi})|M\rangle = \frac{1}{2}(\delta_{N,M+k} + \delta_{N,M-k})$:

$$\langle\pm 1|V|0\rangle = -E_J^{(1)}/2, \quad \langle\pm 2|V|0\rangle = -E_J^{(2)}/4$$

Energy denominators: $E_0^{(0)} - E_N^{(0)} = -4E_C N^2$. Summing contributions ($N = \pm 1, N = \pm 2$):

$$E_0^{(2)} = 2\frac{|-E_J^{(1)}/2|^2}{-4E_C(1)^2} + 2\frac{|-E_J^{(2)}/4|^2}{-4E_C(2)^2} = -\frac{(E_J^{(1)})^2}{8E_C} - \frac{(E_J^{(2)})^2}{128E_C}$$

a.iii) Charge Qubit near $n_g = 1/2$

Degenerate subspace $\{|0\rangle, |1\rangle\}$ near $n_g = 1/2$. Let $n_g = 1/2 + \delta$. Unperturbed energies: $E_0^{(0)} \approx E_C - 4E_C\delta$, $E_1^{(0)} \approx E_C + 4E_C\delta$. Perturbation matrix element: $V_{01} = \langle 0|V|1\rangle \approx -E_J^{(1)}/2$. Hamiltonian matrix (basis $\{|0\rangle, |1\rangle\}$):

$$H \approx \begin{pmatrix} E_C - 4E_C\delta & -E_J^{(1)}/2 \\ -E_J^{(1)}/2 & E_C + 4E_C\delta \end{pmatrix}$$

Effective Hamiltonian ($H_{\text{eff}} = H - E_C I$, $\epsilon_0 = 4E_C\delta = 4E_C(n_g - 1/2)$):

$$H_{\text{eff}} = \begin{pmatrix} -\epsilon_0 & -E_J^{(1)}/2 \\ -E_J^{(1)}/2 & \epsilon_0 \end{pmatrix} = -\epsilon_0\hat{\sigma}_z - \frac{E_J^{(1)}}{2}\hat{\sigma}_x$$

Eigenvalues: $E_\pm = \pm\sqrt{\epsilon_0^2 + (E_J^{(1)}/2)^2}$. Ground state ($E_-$) probability in state $|0\rangle$:

$$P(N=0) = \frac{1}{2}\left(1 + \frac{\epsilon_0}{\sqrt{\epsilon_0^2 + (E_J^{(1)}/2)^2}}\right)$$

(Sign depends on basis ordering/σ_z convention, plot shape is key).

A.2 Part (b): Josephson Dominated Regime ($E_J^{(1)}, E_J^{(2)} \gg E_C$, $n_g = 0$)

Valid for $E_J/E_C \gg 1$.

b.i) Harmonic Oscillator Approximation: Levels and Wavefunctions

Potential $V(\phi) = -E_J^{(1)}\cos\phi - \frac{E_J^{(2)}}{2}\cos(2\phi)$. Expand around $\phi = 0$:

$$V(\phi) \approx V(0) + \frac{1}{2}V''(0)\phi^2 + \frac{1}{24}V^{(4)}(0)\phi^4 + ...$$

$$V(0) = -E_J^{(1)} - E_J^{(2)}/2$$

$$V''(0) = E_J^{(1)} + 2E_J^{(2)} \equiv k$$

$$V^{(4)}(0) = -(E_J^{(1)} + 8E_J^{(2)})$$

Approximate Hamiltonian (HO): $\hat{H}_{HO} = V(0) + 4E_C\hat{N}^2 + \frac{1}{2}k\hat{\phi}^2$. Effective mass $m^* = 1/(8E_C)$, frequency $\omega = \sqrt{k/m^*} = \sqrt{8E_Ck}$. Energy levels: $E_n^{(HO)} = V(0) + \omega(n + 1/2)$. Width parameter: $\alpha = (m^*\omega)^{1/4} = (k/(8E_C))^{1/4}$. Wavefunctions: $\psi_n^{(HO)}(\phi) = N_nH_n(\alpha\phi)e^{-\alpha^2\phi^2/2}$.

b.ii) Probability Density Plot

Probability densities $p_n(\phi) = |\psi_n^{(HO)}(\phi)|^2$ for $n = 0, 1, 2$ using $\alpha^2 = 10$ (for $E_C = (E_J^{(1)} + 2E_J^{(2)})/800$) are plotted in Figure 8.

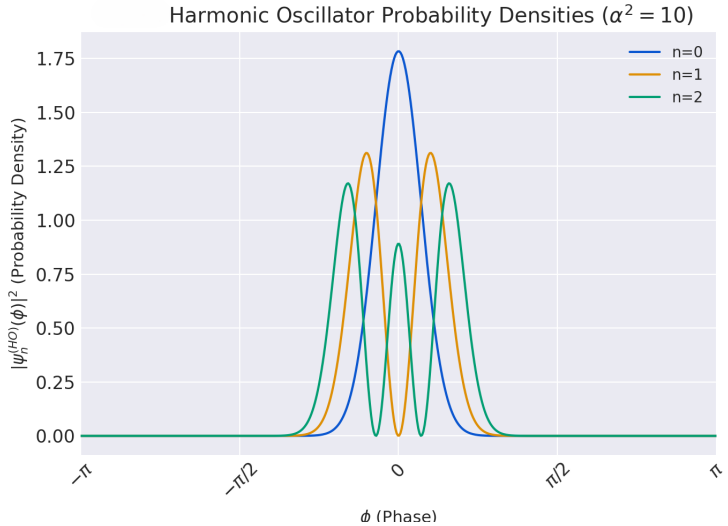

Fig. 8: Approximate HO probability densities $p_n(\phi)$ for $n = 0, 1, 2$ with $\alpha^2 = 10$.

b.iii) Charge Expectation Value and Variance

Ground state average: $\langle\hat{N}\rangle_0 = 0$. Variance: $\Delta N^2 = \langle\hat{N}^2\rangle_0$. Relation to kinetic energy: $\langle KE\rangle_0 = 4E_C\langle\hat{N}^2\rangle_0 = \omega/4$.

$$\langle\hat{N}^2\rangle_0 = \frac{\omega}{16E_C}$$

Using $X = \sqrt{8E_C/k}$: $\omega = \sqrt{8E_Ck} = \sqrt{8E_C(8E_C/X^2)} = 8E_C/X$.

$$\Delta N^2 = \frac{8E_C/X}{16E_C} = \frac{1}{2X}$$

b.iv) Subleading Correction to Energy Levels

Perturbation: $V_{pert} = \frac{1}{24}V^{(4)}(0)\hat{\phi}^4 = -\frac{E_J^{(1)}+8E_J^{(2)}}{24}\hat{\phi}^4$. First-order correction: $E_n^{(1)} = \langle n|V_{pert}|n\rangle$. Expectation value: $\langle n|\hat{\phi}^4|n\rangle = (\frac{4E_C}{\omega})^2(6n^2+6n+3)$.

$$E_n^{(1)} = -\frac{E_J^{(1)}+8E_J^{(2)}}{24}\left(\frac{4E_C}{\omega}\right)^2(6n^2+6n+3)$$

Substituting $\omega^2 = 8E_C(E_J^{(1)}+2E_J^{(2)})$:

$$E_n^{(1)} = -\frac{E_C(E_J^{(1)}+8E_J^{(2)})}{12(E_J^{(1)}+2E_J^{(2)})}(6n^2+6n+3) \equiv -C(6n^2+6n+3)$$

Corrections: $E_0^{(1)} = -3C$, $E_1^{(1)} = -15C$, $E_2^{(1)} = -39C$.

b.v) Interpretation: Are Levels Equidistant?

Energy differences:

$$E_1 - E_0 \approx \omega - 12C$$

$$E_2 - E_1 \approx \omega - 24C$$

Anharmonicity:

$$\alpha_{anh} = (E_2-E_1)-(E_1-E_0) \approx -12C = -E_C\frac{E_J^{(1)}+8E_J^{(2)}}{E_J^{(1)}+2E_J^{(2)}}$$

Since $\alpha_{anh} \neq 0$, levels are not equidistant. If $E_J^{(2)} = 0$, $\alpha_{anh} = -E_C$.

A.3 Part (c): Exactly Solvable Case ($E_J^{(1)} = E_J, E_J^{(2)} = E_J^2/(4E_C)$)

Parameters: $n_g = 0$, $E_J^{(1)} = E_J$, $E_J^{(2)} = E_J^2/(4E_C)$.

Hamiltonian:

$$\hat{H} = 4E_C\hat{N}^2 - E_J\cos(\hat{\phi}) - \frac{E_J^2}{8E_C}\cos(2\hat{\phi}).$$

Exact ground state energy: $E_0 = -E_J^2/(8E_C)$. Unnormalized ground state wavefunction: $\psi_0(\phi) = A\exp(\frac{E_J}{4E_C}\cos\phi)$. Normalization integral:

$$\int_{-\pi}^{\pi}|\psi_0(\phi)|^2 d\phi = 2\pi|A|^2 I_0(E_J/(2E_C)),$$

where I_0 is the modified Bessel function of the first kind. Normalized probability density:

$$p(\phi) = \frac{\exp(\frac{E_J}{2E_C}\cos\phi)}{2\pi I_0(E_J/(2E_C))}$$

This is plotted in Figure 5. Comparison: E_0 matches $E_0^{(2)}$ from Sec. A.1 if $E_J^{(1)} = E_J, E_J^{(2)} = 0$.